Available online at www.sciencedirect.com
ScienceDirect
Journal of Sound and Vibration 321 (2009) 201–219
JOURNAL OF SOUND AND VIBRATION
www.elsevier.com/locate/jsvi

A two-sided interface model for dissipation in structural systems with frictional joints

Jason D. Miller, D. Dane Quinn*

Department of Mechanical Engineering, The University of Akron, Akron, OH 44325-3903, USA

Received 12 October 2007; received in revised form 31 July 2008; accepted 15 September 2008
Handling Editor: S. Bolton
Available online 18 November 2008

Abstract

Modeling mechanical joints in an accurate and computationally efficient manner is of great importance in the analysis of structural systems, which can be composed of a large number of connected components. This work presents an interface model that can be decomposed into a series-series Iwan model together with an elastic chain, subject to interfacial shear loads. A reduced-order formulation of the resulting model is developed that significantly reduces the computational requirements for the simulation of frictional damping. Results are presented as the interface is subject to harmonic loading of varying amplitude. The models presented are able to qualitatively reproduce experimentally observed dissipation scalings. Finally, the interface models are embedded within a larger structural system to illustrate there effectiveness in capturing the structural damping induced by mechanical joints.

1. Introduction

Complex engineering structures are often composed of a multitude of components, connected by mechanical joints and interfaces, which are often give rise to a significant fraction of the overall dissipation observed in the response. This damping is associated with interfacial frictional slip, known as microslip, and is strongly amplitude dependent and hence nonlinear [1–3]. Predictive structural models therefore require an accurate representation of the behavior at and near the interface, giving rise to the experimentally observed nonlinear stiffness and damping characteristics.

The most direct method to represent microslip in a larger structural model is to resolve the interface in a finite element model [4]. Unfortunately, the small length scales required to capture the mechanics of microslip lead to a problem for which the time required to generate a computational solution is prohibitively long [5]. Thus, one is led to search for alternative representations of the dissipation induced by mechanical interfaces with larger structural models. One common technique is to incorporate the observed dissipation into a linear joint model with effective mass, damping and stiffness parameters, which must then be estimated to match experimentally observed results. However, the identified parameters are thus tied to the response of a

*Corresponding author. Tel.: +1 330 972 6302; fax: +1 330 972 6027.
E-mail addresses: jason31@uakron.edu (J.D. Miller), quinn@uakron.edu (D. Dane Quinn).

0022-460X/$ - see front matter © 2008 Elsevier Ltd. All rights reserved.
doi:10.1016/j.jsv.2008.09.037

particular test. As the forcing levels vary the identified parameters can change significantly because of the nonlinear nature of the interface dissipation—the joint model is no longer predictive.

The role of friction and microslip has been incorporated into several nonlinear reduced-order models for the joint based on descriptions of the slip interface in the joint. Menq, Bielak, and Griffin [6] develop a continuum model representing the microslip that arises in frictional dampers. Quinn and Segalman [7] consider a similar model and show that by varying the spatial distribution of the frictional intensity the predicted dissipation is representative of experimentally observed scalings. Discrete models of the interface are often based on combinations of spring-slider elements, as considered by Iwan [8,9]. Sengalman [10] has developed a four parameter Iwan model that is capable of reproducing the qualitative properties of the joint dynamics. Meanwhile, Song, Hartwigsen, McFarland, Vakakis, and Bergman [11] have developed an adjusted Iwan beam element based on a parallel-series Iwan model that can be naturally incorporated into an existing finite element framework. With the proper identification of the model parameters, the adjusted Iwan beam element can be used to capture experimentally observed profiles for the response of jointed structures.

The present work considers a two-sided interface model based on a series-series Iwan model in which the parameters are physically motivated [7]. The model is shown to naturally decompose into an elastic and dissipative component that decouple for time-dependent external forces applied to the joint. This interface model is then incorporated into a larger structural model, following the approach taken in Song, Hartwigsen, McFarland, Vakakis, and Bergman [11]. Once embedded in the structural model the elastic and dissipative components of the joint model couple together through the forces acting on the interface. Finally, this joint model is shown to qualitatively reproduce response features of jointed structures observed experimentally.

2. A two-sided interface model

To begin consider a single series of Iwan elements, made up of n interfaces and $2(n-1)$ masses as shown in Fig. 1. In this model each element is assumed to be identical, with a mass m, and a stiffness k, respectively. The forces f_i and g_i, $i=1,\ldots,n-1$ represent the shear loading applied to the masses in the ith component, while f_0 and g_0 (f_n and g_n) describe the forces acting on the left (right) edge of the interface. In addition, each interface is described through the frictional force σ_i. For this system the equations of motion can be written as

$$m\ddot{x}_i + 2kx_i - k(u_i + u_{i+1}) = f_i, \quad \text{upper masses,} \tag{1a}$$

$$m\ddot{y}_i + 2ky_i - k(v_i + v_{i+1}) = g_i, \quad \text{lower masses,} \tag{1b}$$

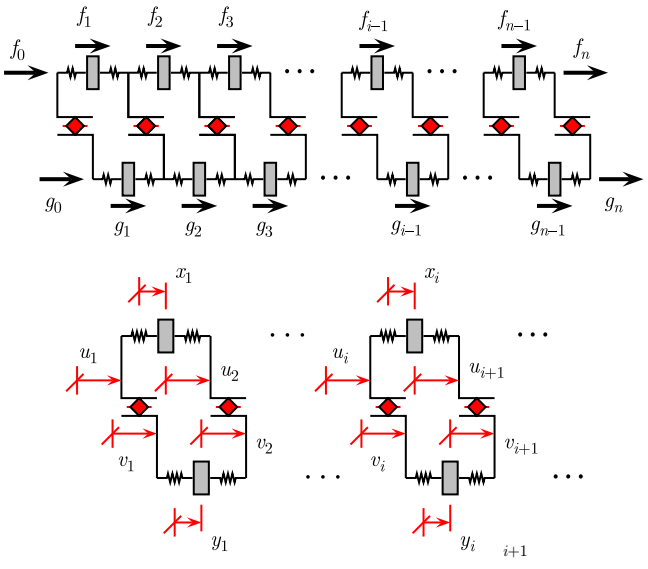

Fig. 1. Discrete model.

$$\begin{aligned}&\sigma_1 + k(x_1 - u_1) + f_0 = 0,\\ &-\sigma_1 + k(y_1 - v_1) + g_0 = 0,\end{aligned} \quad \text{1st slider,} \tag{1c}$$

$$\begin{aligned}&\sigma_i + k(x_{i-1} - 2u_i + x_i) = 0,\\ &-\sigma_i + k(y_{i-1} - 2v_i + y_i) = 0,\end{aligned} \quad i\text{th slider,} \tag{1d}$$

$$\begin{aligned}&\sigma_n + k(x_{n-1} - u_n) + f_n = 0,\\ &-\sigma_n + k(y_{n-1} - v_n) + g_n = 0,\end{aligned} \quad n\text{th slider.} \tag{1e}$$

This two-sided interface problem, in which deformation can arise on either side, is an extension of the study by Pratt and Williams [12] on the steady-state relative motion of two masses with Coulomb friction acting between them. Note that if the interface is characterized by Coulomb friction, then $\sigma_i = -\mu_i \cdot N_i \operatorname{sgn}(\dot{u}_1 - \dot{v}_1)$, where μ_i and N_i are the coefficient of friction and the normal load acting on the ith interface, respectively, and we refer to the product $\mu_i \cdot N_i$ as the frictional intensity. From these equations, and the symmetry of the system, the following coordinates can be identified

$$w_i = \frac{x_i + y_i}{2}, \quad z_i = \frac{x_i - y_i}{2},$$

$$p_i = \frac{u_i + v_i}{2}, \quad q_i = \frac{u_i - v_i}{2}, \tag{2}$$

where (w_i, z_i) and (p_i, q_i) represent the average and relative displacements across the masses and sliders, respectively. With these, the equations describing the evolution of w_i decouple from those on z_i to yield

$$m\ddot{w}_i + 2kw_i - k(p_i + p_{i+1}) = \frac{f_i + g_i}{2}, \tag{3a}$$

$$2k(w_1 - p_1) + (f_0 + g_0) = 0, \tag{3b}$$

$$(w_{i-1} - 2p_i + w_i) = 0, \tag{3c}$$

$$2k(w_{n-1} - p_n) + (f_n + g_n) = 0, \tag{3d}$$

$$m\ddot{z}_i + 2kz_i - k(q_i + q_{i+1}) = \frac{f_i - g_i}{2}, \tag{4a}$$

$$2\sigma_1 + 2k(z_1 - q_1) + (f_0 - g_0) = 0, \tag{4b}$$

$$\sigma_i + k(z_{i-1} - 2q_i + z_i) = 0, \tag{4c}$$

$$2\sigma_n + 2k(z_{n-1} - q_n) + (f_n - g_n) = 0. \tag{4d}$$

In the above equations on w_i and p_i, the interface forces σ_i are absent and the response of this set is independent of the interface. Solving for p_i yields

$$p_1 = w_1 + \frac{f_0 + g_0}{2k}, \tag{5a}$$

$$p_i = \frac{w_{i-1} + w_i}{2}, \tag{5b}$$

$$p_n = w_{n-1} + \frac{f_n + g_n}{2k}. \tag{5c}$$

These can then be returned to the equations for $\ddot{w}_i$ to yield

$$m\ddot{w}_1 + \frac{k}{2}(w_1 - w_2) = \left(\frac{f_0 + g_0}{2}\right) + \left(\frac{f_1 + g_1}{2}\right), \tag{6a}$$

$$m\ddot{w}_i + \frac{k}{2}(-w_{i-1} + 2w_i - w_{i+1}) = \left(\frac{f_i + g_1}{2}\right), \quad i = 2, \ldots, n-2, \tag{6b}$$

$$m\ddot{w}_{n-1} + \frac{k}{2}(-w_{n-2} + w_{n-1}) = \left(\frac{f_{n-1} + g_{n-1}}{2}\right) + \left(\frac{f_n + g_n}{2}\right). \tag{6c}$$

Therefore these equations are equivalent to those describing the response of an elastic chain, as represented in Fig. 2.

The response described by w_i is conservative, so that the dissipation in the system arises solely from the equations on z_i, for which the equations of motion can be written as

$$m\ddot{z}_i + k((z_i - q_i) + (z_i - q_{i+1})) = \frac{f_i - g_i}{2}, \tag{7}$$

with

$$\sigma_1 = -\left(\frac{f_0 - g_0}{2}\right) - k(z_1 - q_1), \tag{8a}$$

$$\sigma_i = -k((z_{i-1} - q_i) + (z_i - q_i)), \quad i = 2, \ldots, n-1, \tag{8b}$$

$$\sigma_n = -\left(\frac{f_n - g_n}{2}\right) - k(z_{n-1} - q_n). \tag{8c}$$

Therefore, these equations represent the dissipative structure shown in Fig. 3, a series-series Iwan system [7]. Notice that the interface forces σ_i do not rely on any specific model for friction, such as Coulomb friction. In addition, these forces need be neither uniform in space nor constant in time. Thus, the decoupling that arises from the coordinate transformation identified above can be achieved for any interfacial friction model. However, in the numerical results that follow, we do assume that interfacial friction is modeled by Coulomb friction, with a constant uniform frictional intensity.

For this component, the dissipative power can be determined as

$$P_d(t) = \sum_{i=1}^{n} \sigma_i(t) \cdot \dot{q}_i(t), \tag{9}$$

so that the work done by the dissipative component, and therefore the total interface model, becomes

$$-D(t) = \int_0^t \sum_{i=1}^{n} \sigma_i(\tau) \cdot \dot{q}_i(\tau)\, \mathrm{d}\tau. \tag{10}$$

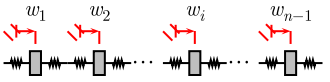

Fig. 2. Elastic component.

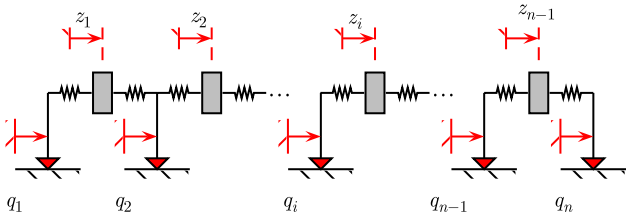

Fig. 3. Dissipative component.

In Quinn and Sengalman [7] a spatially nonuniform frictional intensity is considered and is shown to yield measures for the dissipation that are consistent with experimental data.

3. Model reduction

3.1. Characteristic scales

While the proposed interface model described above is able to represent states of partial slip, its explicit numerical solution is nonetheless restricted by prohibitively small time steps. The characteristic time and length scales of the above interface model serve to guide the model reduction.

To compare interface models of varying size, we scale the inter-element stiffness and mass by the overall static stiffness and total mass of the elastic chain, K_{eq} and M_{eq}, so that

$$k = (n-1)K_{\mathrm{eq}}, \quad m = \frac{M_{\mathrm{eq}}}{2(n-1)}. \tag{11}$$

The lowest characteristic frequency of the interface scales as $\omega_c = \sqrt{K_{\mathrm{eq}}/M_{\mathrm{eq}}}$, so that the largest characteristic frequency scales is

$$\omega_{\max} = \sqrt{\frac{2k}{m}} = 2(n-1)\sqrt{\frac{K_{\mathrm{eq}}}{M_{\mathrm{eq}}}} = 2(n-1)\omega_c. \tag{12}$$

Thus, ω_c describes the characteristic frequency of the interface. If the computational time scale of a larger structural model is also assumed to be characterized by ω_c, the computational time scale with the inclusion of this joint model must be decreased by a factor of n to capture the largest characteristic frequency of the above model. Therefore the inclusion of this chain within larger structural models to represent frictional interfaces remains computationally inefficient. However, based on the decomposition described above, we propose a model reduction strategy based on modal analysis of the elastic chain and a quasi-static treatment of the dissipative component.

A characteristic force for this interface, defined as F_c, can be identified as a frictional intensity associated with the total interface. For example, if the frictional intensity is constant in time, a natural choice for F_c can be chosen as $F_c = \sum_{i=1}^{n}\sigma_i$. For time-dependent frictional intensities, a time average of the total intensity is appropriate. With this, a characteristic length scale of the interface can be identified as

$$L_c = \frac{F_c}{K_{\mathrm{eq}}}, \tag{13}$$

which is associated with the displacement of the joint at the onset of macroslip. These characteristic values, ω_c, F_c, and L_c, can be used as reference values for the response of the interface, so that scaled values of the response can be defined as, for example

$$t^\star = \omega_c t, \quad x^\star = \frac{x(t)}{L_c}, \quad f^\star = \frac{f}{F_c}. \tag{14}$$

In general, the $(\cdot)^\star$ notation indicates the appropriate scaled variables. With the scaled frictional intensity defined as $\sigma_i^\star(t^\star) = \sigma_i(t^\star/\omega_c)/F_c$, the scaled dissipation can be defined as

$$-D^\star(t^\star) = \int_0^{t^\star}\sum_{i=1}^{n}\sigma_i^\star(\tau)\cdot\frac{\mathrm{d}q_i^\star}{\mathrm{d}\tau}(\tau)\,\mathrm{d}\tau \longrightarrow D(t) = (F_cL_c)D^\star(\omega_c t). \tag{15}$$

The model reduction that follows will make use of the characteristic scales identified above, but will be carried out in terms of the original dimensional variables to facilitate the incorporation of this interface model within larger structural systems. However, when isolating the response of the interface alone, the results will be presented relative to these characteristic scales, i.e., in terms of the scaled nondimensional (starred) variables.

3.2. Elastic chain

The response of the elastic chain can be approximated with a Galerkin analysis using only the linear vibrational modes of the chain whose characteristic times are comparable to the time scales of the surrounding structure. In the forced response of the elastic chain the number of modes required to describe the response of the component depends on the characteristic time scale of the forcing—longer time scales require, in general, fewer modes for accurate description.

Retaining only the lowest s linear modes for the elastic chain, denoted as $\boldsymbol{\phi}_i$, $i = 1, \ldots, s$, the response of this component is then given as

$$w_i(t) = \sum_{j=1}^{s} W_j(t)[\boldsymbol{\phi}_j]_i, \tag{16}$$

where the modal amplitudes $W_j(t)$ are approximated by a reduced-order model of the form

$$\hat{\mathbf{M}}\ddot{\mathbf{W}} + \hat{\mathbf{K}}\mathbf{W} = \hat{\mathbf{f}}(t), \tag{17}$$

with

$$\hat{M}_{jk} = \boldsymbol{\phi}_j^{\mathrm{T}}\mathbf{M}\boldsymbol{\phi}_k, \quad \hat{K}_{jk} = \boldsymbol{\phi}_j^{\mathrm{T}}\mathbf{K}\boldsymbol{\phi}_k, \quad \hat{f}(t)_j = \boldsymbol{\phi}_j^{\mathrm{T}}\mathbf{f}(t). \tag{18}$$

3.3. Dissipative chain

In the series-series Iwan chain, the dissipation can be accurately captured by neglecting the mass in each Iwan element, again provided that the time scale of the external loading is sufficiently long—effectively solving for the response of the system quasi-statically. Therefore, a finer mesh of dissipative Iwan elements can be used to describe partial slip states without the computational penalty of prohibitively small time steps required for numerical stability. With $m = 0$ the displacement of z_i is

$$z_i = \frac{f_i - g_i}{4k} + \frac{q_i + q_{i+1}}{2}, \tag{19}$$

so that the equations of motion for the massless dissipative chain can be written as

$$k(q_1 - q_2) = (f_0 - g_0) + \left(\frac{f_1 - g_1}{2}\right) + 2\sigma_1, \tag{20a}$$

$$k(-q_{i-1} + 2q_i - q_{i+1}) = \left(\frac{f_{i-1} - g_{i-1}}{2}\right) + \left(\frac{f_i - g_i}{2}\right) + 2\sigma_i, \quad i = 2, \ldots, n-1, \tag{20b}$$

$$k(-q_{n-1} + q_n) = (f_n - g_n) + \left(\frac{f_{n-1} - g_{n-1}}{2}\right) + 2\sigma_n, \tag{20c}$$

and are representative of the dissipative structure in Fig. 4, a massless series-series Iwan model. The above equations can be written in a compact matrix form as

$$\mathbf{K} \cdot \mathbf{q} = \mathbf{R}, \tag{21}$$

and solved quasi-statically at each time step. In the same spirit of Kim and Kwak [13], Berger et al. [14], and Cocu et al. [15], a complementarity approach was implemented to solve the matrix equations. An initial

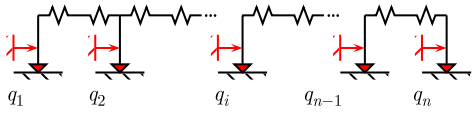

Fig. 4. Massless dissipative component.

assumption array on the slip state of each slider is created a priori to each time step. The slider is assumed to be in a state of stiction, slipping right, or slipping left. Based on this assumption, the state variables describing the elastic and dissipative systems are calculated. Depending on the assumption of slip state, either slider displacements or frictional forces are solved for in the dissipative component of the interface. A solution array is then formulated based on the slip state of each slider at the conclusion of the time step. If the solution and assumption arrays agree the time step is then advanced, else the assumption array is updated according to the solution array and the time step is repeated. This process continues until convergence. However, if the iteration fails to converge, the magnitude of the time step is reduced and the process repeats.

3.4. Reduced-order interface model

From the solution of these two separate subsystems on w_i for the elastic chain and (z_i, q_i) for the dissipative component, the coordinates of the original model can be determined as

$$x_i = w_i + z_i, \quad y_i = w_i - z_i,$$

$$u_i = p_i + q_i, \quad v_i = p_i - q_i. \tag{22}$$

Note that for the massless dissipative chain z_i can be determined in terms of the slider displacements.

In particular, since p_i can be written in terms of the average displacement of the blocks w, the relative displacement across the interface for both models become

$$\begin{aligned} \Delta_1 &= u_n - v_1, \\ &= (w_{n-1} - w_1) + (q_n + q_1) + \left[\frac{(f_n + g_n) - (f_0 + g_0)}{2k}\right], \end{aligned} \tag{23}$$

and

$$\begin{aligned} \Delta_2 &= v_n - u_1, \\ &= (w_{n-1} - w_1) - (q_n + q_1) + \left[\frac{(f_n + g_n) - (f_0 + g_0)}{2k}\right]. \end{aligned} \tag{24}$$

In each expression, the first term represents the deformation of the elastic chain while the second describes contribution from the dissipative component of the response. The final term in each expression arises from the elasticity at each edge of the original model. As the number of interface elements increases, the stiffness increases and this term becomes negligible.

If one is only concerned with the deformation across this element, as described by $\Delta_{1,2}$, then these models are equivalent to a series-series Iwan model with appropriate shear loads, as studied by Quinn and Segalman [7], combined with an elastic chain. The kinetic energy of the system is primarily contained within the elastic chain, while the dissipation due to the interface is solely described by the series-series Iwan system. In the development of these decoupled subsystems, the degree-of-freedom of each component is related, although in the model reduction scheme described above the degree-of-freedom of the elastic and dissipative components need not be related.

We consider the response and energy dissipation of this interface element relative to the characteristic scales identified in Section 3.1. In the simulations below the frictional intensity is assumed to be spatially uniform and constant in time, while the interface is subjected to direct time-dependent loading. Specifically, the external forces acting on the element are chosen as

$$f_0(t) = 0, \quad f_n(t) = F_0 \sin(\omega t),$$

$$g_0(t) = -F_0 \sin(\omega t), \quad g_n(t) = 0. \tag{25}$$

Relative to the characteristic force F_c, the system experiences macroslip when $F_0^\star \equiv F_0/F_c = \frac{1}{2}$ and recall that as n varies the mass and stiffness scale as given in Eq. (11).

3.4.1. Dissipative component

In the dissipative component, described by Eqs. (7) and (21), the response is governed by the propagation of slip interfaces, transitions between intervals of opposing directions for the frictional contact force [7]. Moreover, for the series-series Iwan component, the dissipation per cycle as a function of forcing amplitude follows a power-law scaling under general assumptions on the frictional intensity. Finally, due to the decoupling described above, any conclusions drawn from the dissipative component also hold for the original two-sided interface model as well, under the corresponding time-dependent external loads.

From the discrete dissipative system given by Eq. (7), the dissipation per forcing cycle is illustrated in Fig. 5 for $n = 40$ as the forcing amplitude $F_0^\star$ varies. Here the scaled dissipation is shown when $\omega^\star \equiv \omega/\omega_c = \pi/15$, so that the excitation frequency is chosen well below the characteristic frequency of the interface ω_c. Nonetheless, the computational time scale is limited by the characteristic frequency $\omega_{\max} = 2(n-1)\omega_c$ imposed by the discretization. However, we expect the interface to respond almost quasi-statically to the applied load. The large open circles describe the numerical simulations of the original model (with mass) using the built-in numerical solver `ode45` within MATLAB. The smaller filled triangles, which are almost coincident with the original model, represent the dissipation arising from the complementarity formulation of the dissipative chain. Finally, for comparison, the prediction from the quasi-static continuum limit, described by Quinn and Segalman [7], is shown as the solid line and can be expressed as

$$D^\star_{\text{continuum}} = \tfrac{8}{3}(F_0^\star)^3. \tag{26}$$

As expected, the dissipation follows a power-law scaling with exponent $m \sim 3$ and Quinn and Segalman have shown that this exponent varies with the spatial distribution of the normal traction, or equivalently the frictional intensity μ_i [7]. The numerical simulations experience macroslip as the forcing amplitude increases above $F_0^\star = 0.50$, and below $F_0^\star \sim 0.025$ the system dissipates no energy due to the discrete description of the interface. As the frictional intensity varies, the resulting dissipation per forcing cycle is shown in Fig. 6.

Thus the dissipation of the Iwan chain is well represented by the complementarity approach, in which the mass is neglected. However, the computational effort required for the later approach is significant reduced, compared to the formulation of the dissipative chain with mass. Fig. 7 shows the computational time required to simulate three complete forcing cycles with $\omega^\star = \pi/15$ and for a forcing amplitude of $F_0^\star = 0.25$ on each side of the interface, which is equivalent to 50% of the load required to initiate macroslip. The computational time required for the complementarity approach is at least an order of magnitude less than that required for the differential formulation. As seen in Fig. 8, the dissipation per cycle $D^\star$ predicted by the reduced-order formulation converges as n increases.

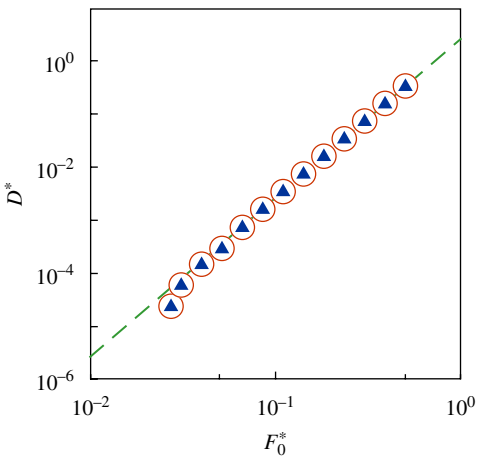

Fig. 5. Numerical simulations of the discrete dissipative component ($n = 40, \omega^\star = \pi/15$). The open circles represent original Iwan with mass while the filled triangles describe the complementarity formulation. Finally, the solid line is the continuum prediction $D^\star = \frac{8}{3}(F_0^\star)^3$, based on Quinn and Segalman [7].

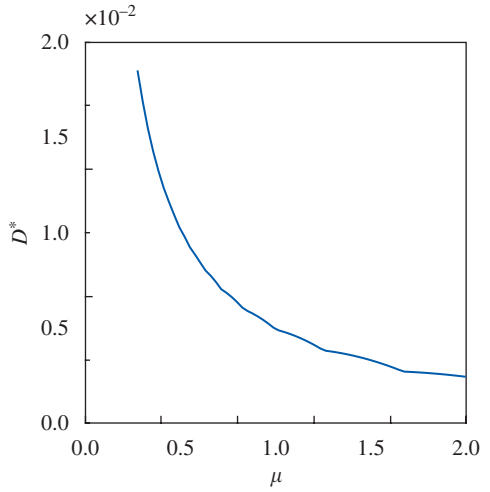

Fig. 6. Total nondimensional dissipation per cycle $D^\star$ in the reduced-order model with increasing frictional intensity μ ($F_0^\star = 0.25, \omega^\star = \pi/15$).

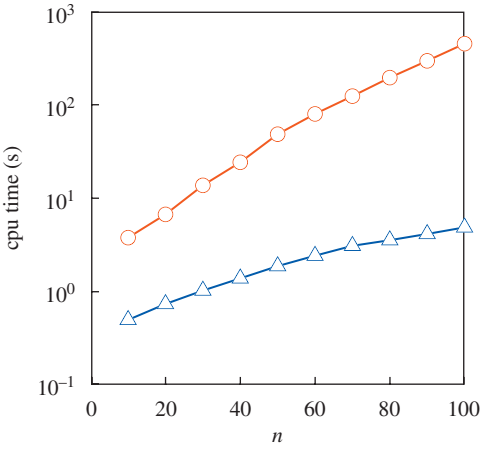

Fig. 7. CPU time required for solution of the Iwan dissipative chain as model order (n) varies ($F_0^\star = 0.30, \omega^\star = \pi/15$). The open circles indicate the original differential formulation while the triangles denote the CPU time required for the complementarity approach.

3.4.2. *Interface response*

With $n = 40$, so that there exist 40 slip locations across the interface, the total steady-state response across the two-sided interface model, $\Delta_1^\star$, is shown in Fig. 9. Specifically, the response for the original differential formulation is shown in Fig. 9a while the response of the reduced-order model is depicted in Fig. 9b. In each panel the contribution from each component is shown, in addition to the total relative displacement across the interface. The time interval shown corresponds to a single forcing cycle after the decay of the transient response. While the displacement across the elastic component is smooth, as expected, the dissipative component undergoes stick–slip dynamics. The scaled displacement is shown as a function of the scaled applied force in Fig. 10a, exhibiting significant hysteresis per loading cycle and therefore energy dissipation. The small amplitude fluctuations seen in the hysteresis loop arise from the high frequency modes in the elastic component.

Comparing the difference between the two formulations, the error in the total displacement between the differential and reduced-order formulation is shown in Fig. 11 as the model size n increases. In the reduced-order formulation $s = 10$ modes have been retained in the elastic component. As the resolution of the interface

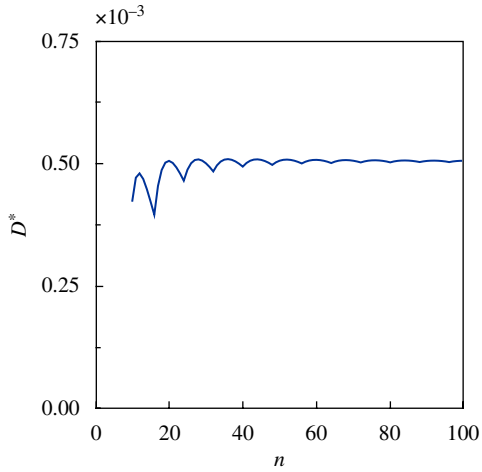

Fig. 8. Total nondimensional dissipation per cycle $D^\star$ in the reduced-order model, with increasing model size n ($F_0^\star = 0.25, \omega^\star = \pi/15$).

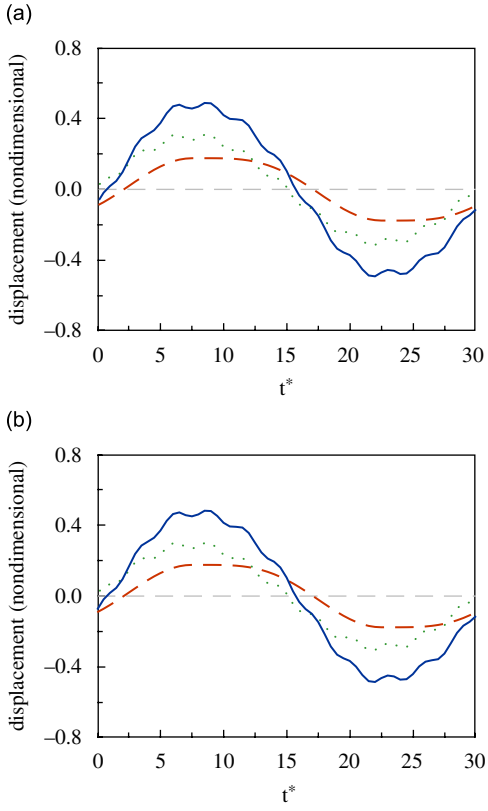

Fig. 9. Numerical response across the interface to harmonic loads $n = 40, F_0^\star = 0.50, \omega^\star = \pi/15$) simulations of the discrete dissipative component. In each panel the solid curve describes the total displacement across the interface $\Delta_1^\star(t)$ —, with $(q_n^\star + q_1^\star)$ - - -, $(w_{n-1}^\star - w_1^\star)$ ..... : (a) differential interface and (b) reduced-order interface.

increases the reduced-order model approaches the differential formulation. Finally, the computational time required for the numerical solution of these two formulations is illustrated in Fig. 12. The computational time required for the original differential formulation appears to grow at a much faster rate than that of the

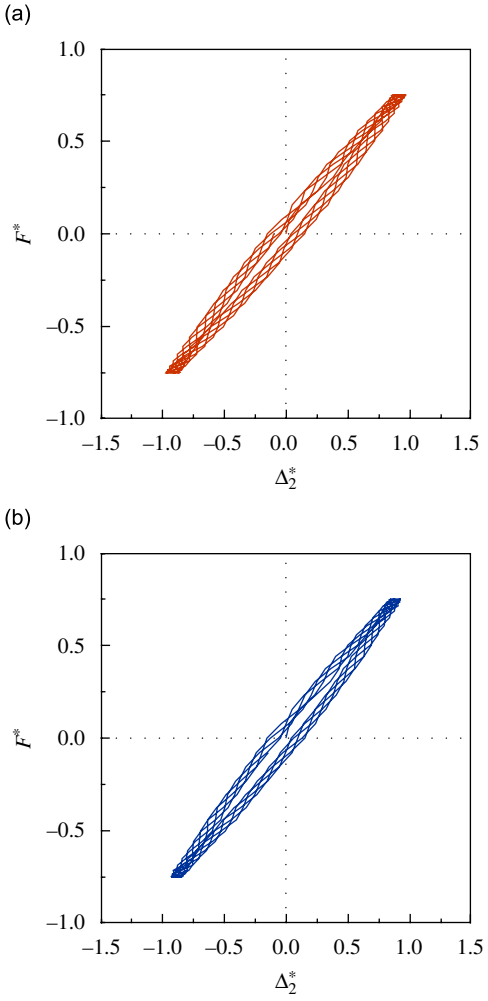

Fig. 10. Hysteresis curve ($n = 32, T^\star = 30 = 2\pi/\omega^\star, F_0^\star = 0.75$): (a) differential interface and (b) reduced-order interface.

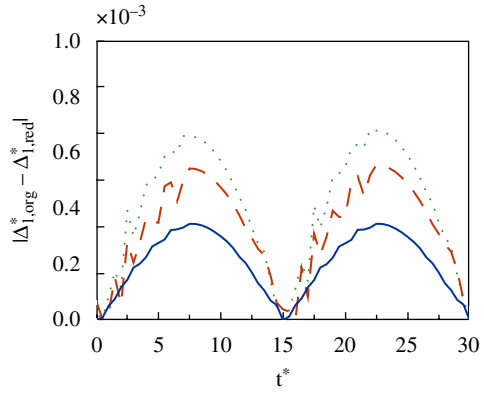

Fig. 11. Difference in total displacement $\Delta_1^\star$ between the differential and reduced-order formulation of the interface model ($s = 10$, $F_0^\star = 0.30, \omega^\star = \pi/15$) $n = 100$ —, with $n = 40$ ---, $n = 20$ .....

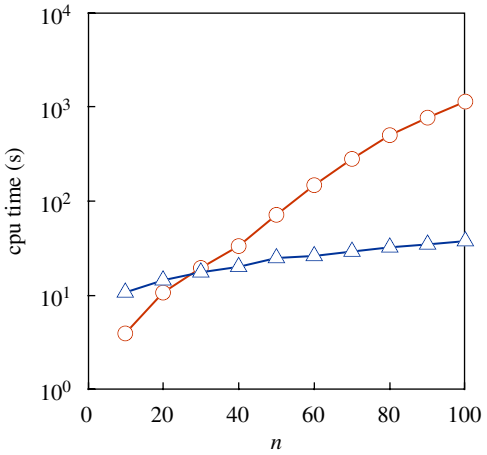

Fig. 12. CPU time required for solution of the full interface model as model order (n) varies ($F_0^\star = 0.50, \omega^\star = \pi/15$). The open circles indicate the original differential formulation while the triangles denote the CPU time required for the reduced-order model ($s = 4$).

reduced-order model and for $n = 100$ requires two orders of magnitude longer to simulate. In addition to the computational efficiency of the complementarity formulation, the modal analysis applied to the elastic chain is significantly more efficient than the simulation of the original n-degree-of-freedom elastic chain. Again, in these results, ω_c, L_c, and F_c, the characteristic values of the interface, have been used to scale the response so that the observed behavior can be interpreted as relative to these time, length, and force scales described in Section 3.1.

4. Structural response

The ability of this interface model to represent structural damping can best be evaluated within a larger structural system. As illustrated in Fig. 13, a frictional interface joining the two rods undergoing longitudinal deformation is considered. In the monolithic structure (no joint), we consider the system to be represented by an elastic chain of r discrete spring–mass elements. Here each spring and mass is assumed to be identical, with mass $\hat{M} = M/r$ and stiffness $\hat{K} = r\,K$, so that the total mass of the system is M and the equivalent static stiffness of the rod is K. Identifying the characteristic force as the total frictional intensity of the interface F_c, this system can be nondimensionalized with the characteristic frequency $\sqrt{K/M}$, so that $\tau \equiv \sqrt{K/M}t$, and characteristic length F_c/K.[1] Note however that the characteristic scales described in Section 3.1 are distinct from this nondimensionalization of the structure. The former is based on the interface itself while the latter is relative to the overall structural system.

With the nondimensional displacement of the ith mass described by $a_i(\tau)$, the nondimensional equations of motion for the longitudinal deformation can be written as

$$\frac{1}{r}a_1'' + r(2a_1 - a_2) = 0, \tag{27a}$$

$$\frac{1}{r}a_i'' + r(-a_{i-1} + 2a_i - a_{i+1}) = 0, \quad i = 2, 3, \ldots, r-1, \tag{27b}$$

$$\frac{1}{r}a_r'' + r(-a_{r-1} + 2a_r) = F(\tau), \tag{27c}$$

where $\mathrm{d}/\mathrm{d}\tau \equiv (\cdot)'$ and the chain is subject to the (nondimensional) external load $F(\tau)$. Notice that the monolithic structure contains no dissipative terms so that the total energy is conserved. In the presence of the

[1]The models for both the monolithic and jointed structures will be scaled by the same characteristic length.

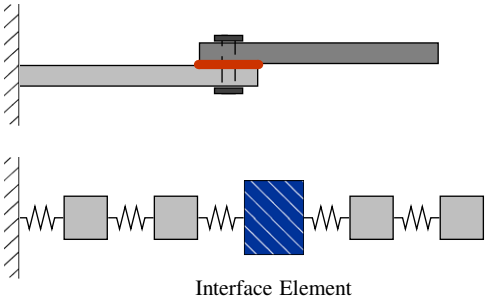

Fig. 13. One-dimensional elastic rod with frictional interface.

interface the ℓth mass is replaced by an Iwan interface element as described above. In this nondimensional structural system, the frictional intensity is uniform so that $\mu_i = \mu/n$, and the overall mass and static stiffness of the interface is $M_{\text{eq}} = 1/r$ and $K_{\text{eq}} = r$ (cf., Section 3.1). This procedure follows from the incorporation of an adjusted Iwan beam element into an elastic beam by Song et al. [11]. Away from the joint, the equations governing the response of the elements are unchanged. However, near the interface the equations governing $a_{\ell-1}$ and $a_{\ell+1}$ become

$$\frac{1}{r}a''_{\ell-1} + r(a_{\ell-1} - a_{\ell-2}) = -g_0(\tau), \tag{28a}$$

$$\frac{1}{r}a''_{\ell+1} + r(-a_{\ell+2} + a_{\ell+1}) = -f_n(\tau), \tag{28b}$$

where $g_0(\tau)$ and $f_n(\tau)$ represent the coupling between the Iwan interface element and the surrounding chain. These forces are described as

$$g_0(\tau) = 2r(a_{\ell-1} - v_1) = \frac{2r}{\left(1 + \dfrac{1}{n-1}\right)}(a_{\ell-1} - (w_1 - q_1)), \tag{29a}$$

$$f_n(\tau) = 2r(a_{\ell+1} - u_n) = \frac{2r}{\left(1 + \dfrac{1}{n-1}\right)}(a_{\ell-1} - (w_1 + q_n)), \tag{29b}$$

and $f_0(\tau) = g_n(\tau) \equiv 0$. The quantities w_1, q_1, w_{n-1}, and q_n represent the elastic and dissipative coordinates used within the interface model described above, and are valid when considering either the conventional, or the massless Iwan interface. Finally, the total dissipation in the interface $D(\tau)$ is defined as in Eq. (10).

Thus the two-sided model can be naturally incorporated into larger structural dynamics models through the above described procedure. In addition, with the model reduction procedure described above the computational requirements for its solution can be significantly reduced when compared to the solution of the original model. Recalling the discussion in Section 3.1, in this nondimensional model the characteristic time scale of the joint is $\omega_c = r$, while the characteristic length scale for the joint is $L_c = 1/r$. We note that the response of the elastic and dissipative decomposed components are only coupled through their interaction with the surrounding system via the forces $f_n(\tau)$ and $g_0(\tau)$. In the numerical simulations that follow, the linear structure is composed of $r = 10$ elements.

4.1. Transient response

The transient response of the structure is initiated with a modulated harmonic excitation of the form

$$F(\tau) = \begin{cases} \delta\left[4\dfrac{\tau}{3T}\left(1 - \dfrac{\tau}{3T}\right)\right]\sin\left(\dfrac{2\pi}{T}\tau\right), & 0 \leqslant \tau < 3T, \\ 0, & \tau \leqslant 3T, \end{cases} \tag{30}$$

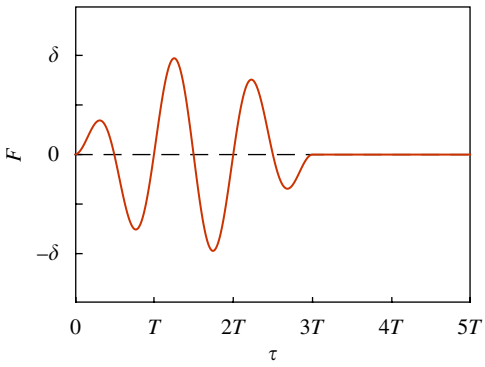

Fig. 14. Transient excitation profile (nondimensional).

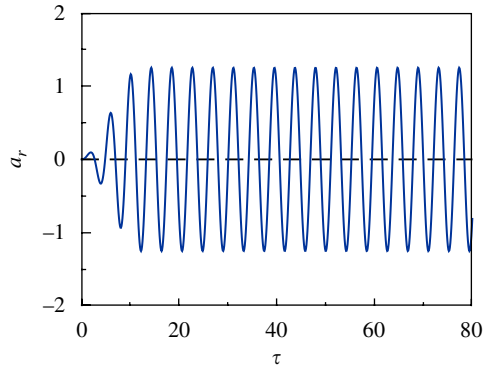

Fig. 15. Nondimensional displacement a_r of the monolithic structure; $\delta = 0.25$ ($r = 10, j = 6, n = 20$).

as illustrated in Fig. 14. Thus the excitation persists for three periods, with the period chosen as $T = 4$, which corresponds to the fundamental period of an elastic rod. In Fig. 15 the response of the monolithic rod (without the interface) is shown when subjected to the above transient loading with zero initial conditions. In the absence of the dissipative interface, once the excitation vanishes the energy in the free response is conserved and the amplitude of the vibrations does not decay.

In the structure, replacing the middle element ($j = 6$) with a differential Iwan interface as developed above, the response of the structure slowly decays in amplitude due to energy dissipation in the interface, here composed of $n = 20$ slip locations. In Fig. 16 the displacement of the free end of the linear chain is shown. Also, a uniform frictional intensity is assumed with $\mu_i = 1.00/n$ while the amplitude of the excitation is chosen to be $\delta = 0.25$. In Fig. 16a the response is shown with the conventional interface formulation while in Fig. 16b the response is shown with the inclusion of the reduced-order model developed above. The the reduced-order model $s = 4$ modes have been retained in the elastic component while the dissipative component is solved quasi-statically. Note that these responses are almost identical.

Although both the conventional and reduced-order interface models can describe the dissipation arising from the frictional slip, the computational requirements for these two models is significantly different. In Fig. 17 the CPU time required for a transient simulation of 40 time units is shown for the conventional and reduced-order interface models as the number of slip locations n and the number of retained elastic modes s vary. This computational time is obtained directly from MATLAB using the internal variable `cputime`. For comparison the CPU time for the monolithic rod is also shown. In Fig. 17a the CPU time is shown as the number of slip locations varies, with $s = 4$. As the order n of the interface increases, the computational time required for the conventional interface grows significantly faster than that of the reduced-order interface

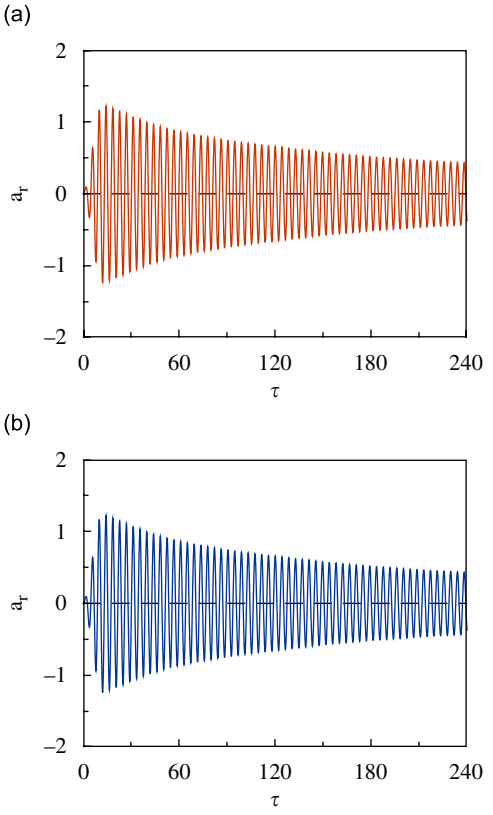

Fig. 16. Nondimensional displacement a_r of the jointed structure; $\delta = 0.25$, $\mu = 1.00$ ($r = 10, j = 6, n = 20$): (a) differential interface and (b) reduced-order interface.

model. For comparison the CPU time required for the simulation of the monolithic structure was 1.9 time units.

In contrast, as shown in Fig. 17b, for fixed $n = 50$, as the number of elastic modes retained increases up to n, the CPU time of the reduced-order model increases. In fact, due to the overhead associated with the modal analysis of the elastic component, for sufficiently large n the computational requirements of the reduced-order model exceed that of the conventional formulation, which is shown as the thin dashed line. However, for small s the computational savings are significant. From this it can be concluded that the computational requirements associated with the elastic component of the interface model, which are reduced as s decreases, serve to limit the efficiency of the reduced-order model. However, the error induced by eliminating these higher-order modes is minimal as illustrated by the response of the rod shown previously in Fig. 16.

The dissipation arising from the frictional interface can be characterized through the decrease in the amplitude of the observed transient response, which from examination of Fig. 16 appears to decay exponentially. Recall that an exponentially decaying function $a(\tau) = a_0 \exp(-\eta\tau)$ can be written as $a(\tau) = \exp(\ln(a_0) - \eta\tau)$. Therefore the slope of $\ln(a(\tau))$ should describe the exponential decay rate for the function. In the transient response of the structural model, the amplitude of the response is identified as the local maximum of the displacement at the free end of the chain, that is $A_i = a_r(\tau_i)$, when $a_r'(\tau_i) = 0$. The slope, and hence the exponential decay rate, is then calculated based on a central difference approximation

$$\eta_i = \frac{\ln(A_{i+1}) - \ln(A_{i-1})}{\tau_{i+1} - \tau_{i-1}}. \tag{31}$$

As seen in Fig. 18, the exponential decay rate as calculated in the above manner is not constant, as would be expected for a linear structure. Instead, as illustrated in Fig. 18a, as the amplitude A_i decreases the identified

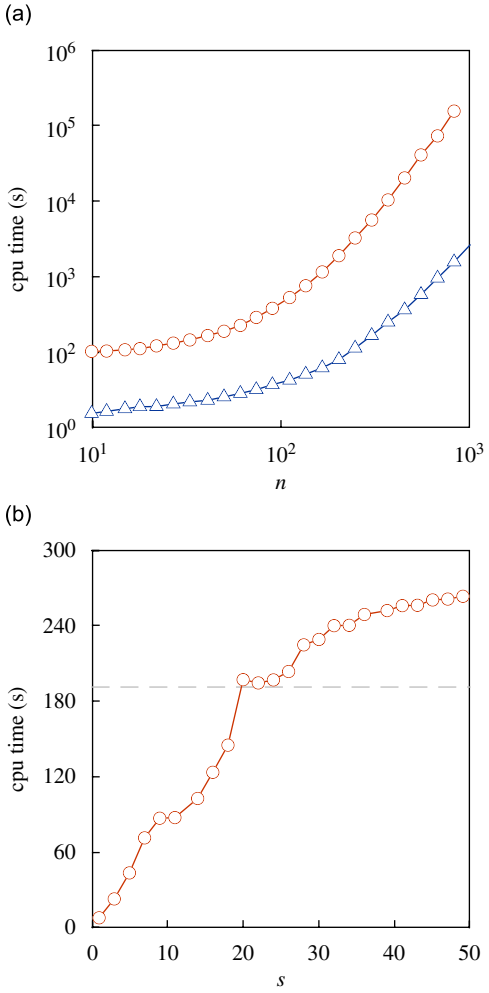

Fig. 17. Computational time required to simulate 40 time units ($r = 10, j = 6, \delta = 0.25, \mu = 1.00$): (a) $s = 4$, open circles—differential interface, triangles—reduced-order interface and (b) $n = 50$.

value of η_i decreases as well. In addition, in Fig. 18b, the exponential decay rate is shown against the amplitude itself, so that the dependence of the dissipation on the amplitude is clear.

4.2. Harmonic excitation

The forced response of the system is generated with an excitation of the form

$$F(\tau) = \begin{cases} \delta\left[\dfrac{\tau}{10(2\pi/\omega)}\left(2 - \dfrac{\tau}{10(2\pi/\omega)}\right)\right]\sin(\omega\tau), & 0 \leqslant \tau < 10\left(\dfrac{2\pi}{\omega}\right), \\ \delta\sin(\omega\tau), & \tau \leqslant 10\left(\dfrac{2,\pi}{\omega}\right), \end{cases} \tag{32}$$

as shown in Fig. 19. The forcing amplitude grows quadratically in time for 10 periods, leading to a stationary harmonic forcing with (nondimensional) frequency ω. In addition, the rod is initially stationary and undeformed. The steady-state amplitude of the response A_{ss} is determined by simulating the structural system for a minimum of 20 forcing cycles, and then estimating the steady-state amplitude of the response from the response based on A_i.

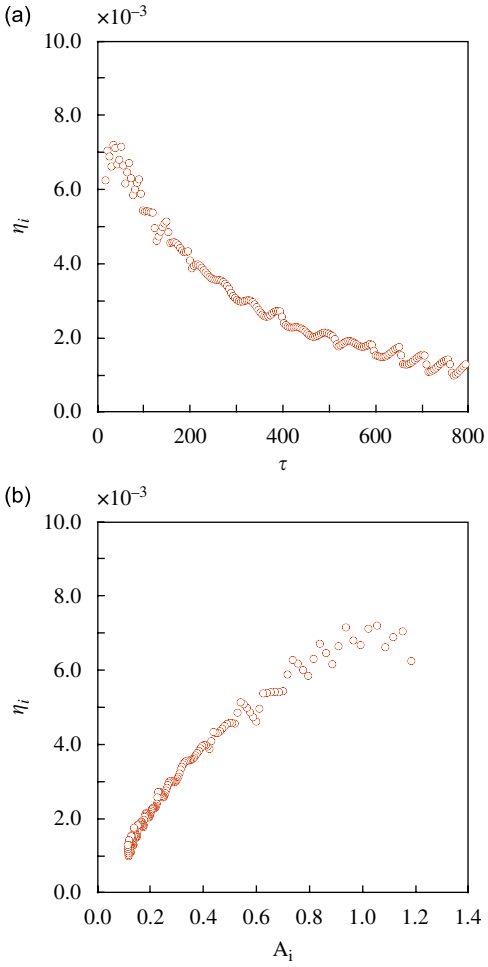

Fig. 18. Exponential decay rate η_i as identified from simulation (cf., Eq. (31)), reduced-order interface ($r = 10, j = 6$; $n = 40, s = 4, \delta = 0.25, \mu = 1.00$): (a) η_i vs. τ and (b) η_i vs. A_i.

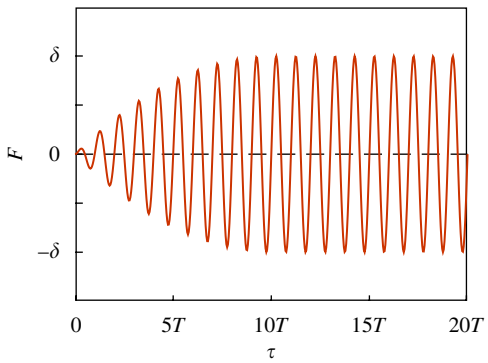

Fig. 19. Harmonic excitation profile (nondimensional), $T = 2\pi/\omega$.

For nonconservative linear structural systems the dissipation per cycle induced by the damping scales quadratically with the external forcing amplitude. In contrast, the dissipation per cycle from the structural interface is shown in Fig. 20. The frequency of the external forcing is chosen to be $\omega = \pi/8$, which is

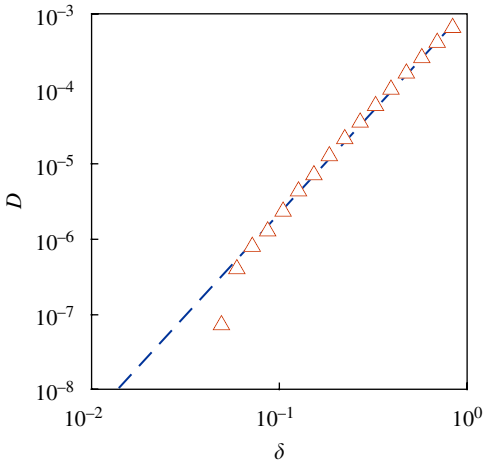

Fig. 20. Dissipation per forcing cycle, reduced-order interface ($r = 10, j = 6, n = 40, s = 4, \mu = 1.00, \omega = \pi/8$).

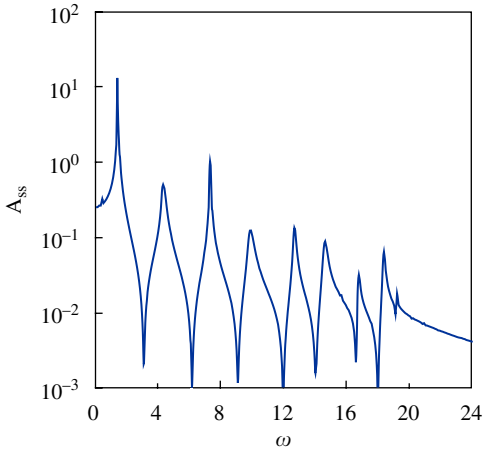

Fig. 21. Response amplitude vs. forcing frequency, reduced-order interface ($r = 10, j = 6, n = 40, s = 4, \delta = 0.25, \mu = 1.00$).

one-quarter of the frequency associated with the fundamental mode of a continuum rod. Below $\delta \sim 0.0450$, the response dissipates no energy, as the loading on the interface is unable to overcome the discretized representation of the frictional contact. Based on the response for which $D > 10^{-6}$, above the effects of the discretization, the dissipation follows a power-law scaling with a fitted exponent of $m \sim 2.72$, shown as the thin dashed line in the figure. Notice that the observed dissipation slope for the structure differs from the slope of three observed when considering the interface alone (cf., Fig. 5)—the dissipation induced in the structure depends not only on the properties of the interface but the dynamics of the structure as well [16]. In addition, as shown in Fig. 21, when the excitation frequency ω is varied with fixed forcing amplitude, the amplitude of the response A_{ss} shows the effect of the induced damping over the range of excitation frequencies.

5. Conclusions

An interface model has been presented that naturally allows for both energy dissipation and elasticity in the joint, and has been shown to capture the structural damping that arises from microslip. The model can be decomposed into a series-series Iwan system, together with an elastic chain subject to tangential loads. Based on this novel decomposition, a reduced-order model was formulated that exhibits significant computational

advantages, yet nonetheless captures the energy dissipation within the interface. The direct investigation of the energy dissipation in the model produced dissipation scalings that are consistent with experimentally observed results. Further, the model was incorporated into a larger structural system. Of course, implementation of this or any reduced-order model will require some experimental tests for validation and identification of the parameters. However, the parameters required by this model are physically motivated. Future directions will include frictional intensities that vary in both time and space and well as the implementation of such models into the response of more complicated structures.

Acknowledgments

This material is based upon work supported by Sandia National Laboratories through Contract number 193122, Dr. Daniel Segalman, Project Director. The authors would like to thank Dr. Segalman and Prof. Ed Berger of the University of Virginia for many helpful discussions. Finally, comments made by the reviewers and editors have greatly enhanced the clarity of the presentation.

References

[1] R.D. Mindlin, H. Deresiewicz, Elastic spheres in contact under varying oblique forces, *Journal of Applied Mechanics—Transactions of the ASME* 20 (1953) 327.
[2] L. Gaul, J. Lenz, Nonlinear dynamics of structures assembled by bolted joints, *Acta Mechanica* 125 (1997) 169–181.
[3] R.A. Ibrahim, C.L. Pettit, Uncertainties and dynamic problems of bolted joints and other fasteners, *Journal of Sound and Vibration* 279 (3–5) (2005) 857–936.
[4] J. Mackerle, Finite element analysis of fastening and joining: a bibliography (1990–2002), *International Journal of Pressure Vessels and Piping* 80 (4) (2003) 253–271.
[5] J.L. Dohner, On the development of methodologies for constructing predictive models of structures with joints and interfaces, Technical Report SAND2001-0003P, Sandia National Laboratories, 2001.
[6] C.-H. Menq, J. Bielak, J.H. Griffin, The influence of microslip on vibratory response, part I: a new microslip model, *Journal of Sound and Vibration* 107 (2) (1986) 279–293.
[7] D.D. Quinn, D.J. Segalman, Using series–series Iwan-type models for understanding joint dynamics, *Journal of Applied Mechanics—Transactions of the ASME* 72 (2005) 778–784.
[8] W.D. Iwan, A distributed-element model for hysteresis and its steady-state dynamic response, *Journal of Applied Mechanics—Transactions of the ASME* 33 (1966) 893–900.
[9] W.D. Iwan, On a class of models for the yielding behavior of continuous and composite systems, *Journal of Applied Mechanics—Transactions of the ASME* 89 (1967) 612–617.
[10] D.J. Segalman, A four-parameter Iwan model for lap-type joints, Technical Report SAND2002-3828, Sandia National Laboratories, 2002.
[11] Y. Song, C.J. Hartwigsen, D.M. McFarland, A.F. Vakakis, L.A. Bergman, Simulation of dynamics of beam structures with bolted joints using adjusted Iwan beam elements, *Journal of Sound and Vibration* 273 (2004) 249–276.
[12] T.K. Pratt, R. Williams, Non-linear analysis of stick/slip motion, *Journal of Sound and Vibration* 74 (4) (1981) 531–542.
[13] J. Kim, B. Kwak, Dynamic analysis of two-dimensional frictional contact by linear complementarity problem formulation, *International Journal of Solids and Structures* 33 (1996) 4605–4624.
[14] E.J. Berger, M.R. Begley, M. Mahajani, Structural dynamic effects on interface response: formulation and simulation under partial slipping conditions, *Journal of Applied Mechanics—Transactions of the ASME* 67 (2000) 785–792.
[15] M. Cocu, E. Pratt, M. Raous, Formulation and approximation of quasistatic frictional contact, *International Journal of Engineering Science* 34 (7) (1996) 783–798.
[16] M. Heinstein, D.J. Segalman, Bending effects in the energy dissipation of bolted interfaces, Presented at the *2001 ASME Design Engineering Technical Conferences*, Pittsburgh, PA, September 9–12, DETC2001/VIB-21517, 2001.